https://doi.org/10.1016/j.matdes.2018.08.040

Rejuvenation by weakening the medium range order in $Zr_{46}Cu_{46}Al_8$ metallic glass with pressure preloading: A molecular dynamics simulation study

S.D. Feng [a, b], K.C. Chan [a,*], L. Zhao [a], S.P. Pan [a, c], L. Qi [b], L.M. Wang [b, *], R.P. Liu [b]

[a] *Advanced Manufacturing Technology Research Centre, Department of Industrial and Systems Engineering, The Hong Kong Polytechnic University, 999077, Hong Kong.*

[b] *State Key Laboratory of Metastable Materials Science and Technology, Yanshan University, Qinhuangdao 066004, China*

[c] *College of Materials Science and Engineering, Taiyuan University of Technology, Taiyuan, 030024, China*

Submitted to

Materials & Design

As a full paper

* Corresponding author.
E-mail & Tel.: kc.chan@polyu.edu.hk; +852-27664981 (K.C. Chan),
limin_wang@ysu.edu.cn; +86-335-8074545 (L.M. Wang).

Abstract

Rejuvenation is the structural excitation of metallic glasses that can significantly increase the enthalpy and free volume. Here, the rejuvenation in $Zr_{46}Cu_{46}Al_8$ metallic glasses with pressure preloading was studied by molecular dynamics simulation. As the strain gradually increases, high-density deformation units in different regions are formed in the rejuvenated $Zr_{46}Cu_{46}Al_8$ metallic glass with pressure preloading, but they do not form the shear bands that cause brittle fracture. In terms of the microstructure, the pressure preloading increases the degree of the short range order, but decreases the medium range order. *3-atom* connections in the medium range order of icosahedra and other clusters are proposed to represent the level of rejuvenation. The decrease of *3-atom* connections in the medium range order can lower the energy barrier and decrease the elastic modulus, improving the level of the rejuvenation. With the weakening of the *3-atom* connections, the rejuvenated metallic glass possesses the features of high density, high energy, high Poisson's ratio, high defects and low localization. These findings open an avenue to evaluate the level of rejuvenation and provide a strong foundation for metallic glass design.

Keywords: metallic glass; rejuvenation; pressure; plasticity; molecular dynamic simulation

1. Introduction

Metallic glasses (MGs), regarded as “green” materials, have non-directional metallic bonds that makes them very different from traditional glasses [1-3]. In particular, brittle fracturing is a fatal flaw in the application of MGs as structural

materials [4-7]. Due to structural softening, shear bands are the preferred positions for plastic flow, and usually a single shear band can lead to ultimate brittle fracture [8-12]. In order to improve the reliability of MGs in engineering applications, a wide range of research has been carried out to prevent brittle fracture [13-16]. At room temperature and normal strain rate, rejuvenated MGs present good deformation ability [17]. Unlike aging, rejuvenation is the structural excitation of MGs, which can significantly increase the enthalpy and free volume [18-22]. Rejuvenating the glass structure to restore flexibility can facilitate bonding-switching to render shear transformations throughout the glass without strain localization in the narrow shear bands [23, 24]. Therefore, without loss of strength and stiffness, achieving a high rejuvenated status and preventing brittle fracture are the keys to extend the applications of MGs.

There are many ways to rejuvenate MGs. Cryogenic thermal cycling makes MGs more disordered and results in a higher energy state, leading to rejuvenation [25-28]. Thermo-mechanical creep can achieve rejuvenation when the stress exceeds a threshold [29]. Elastostatic loading and deformation can also activate rejuvenation [30-32]. Ion irradiation can induce rejuvenation by increasing the free-volume content, achieving shear band intersections in MGs [33]. Some mechanical methods, such as high-pressure torsion, notched constraining and shot peening, can achieve rejuvenation in MGs [34-38].

Pressure can affect many properties of MGs, such as glass transition [39], phase transition [40], crystallization [41], corrosion [42] and deformation [43]. Because of the rapid cooling process, MGs have a large amount of atomic scale free volume [44].

Pressure can induce changes in the microstructure and energy state [45], so that MGs can reach a rejuvenation state, which motivates us to explore the plastic deformation of rejuvenated MGs prepared under pressure. For example, Wang et al. showed that high pressure annealing makes the microstructure change in the “negative flow unit” with a higher packing density, leading to the bulk MGs achieving high energy storage [46]. By a pressure-mediated pathway, Ding et al. found that Cu-Zr MGs exhibit anomalous structure-property relationships in which the energy of the MGs is high, accompanied by an increase in atomic density and icosahedra [47]. Zeng et al. observed that pressure can cause a polyamorphous MG to exhibit elastic anomalies in sonic velocity, volume modulus and Poisson's ratio during the polyamorphic transition [48]. It becomes important to clarify the influence of pressure on the heterogeneity of the microstructure and establish the relationship between the local microstructure and rejuvenation through the pressure effect. Nevertheless, the correlation between the characteristics of the rejuvenation and the atomic structure, the kinds of atomic connections responsible for the main feature of the rejuvenation, and the deformation mechanism under pressure remain elusive. Up to now, proper understanding of the rejuvenation of MGs prepared by pressure preloading is still lacking at the atomic level.

Compared to experimental instruments, computer simulation provides a unique perspective for examining the atomic scale processes in materials and is widely used to reveal the microstructure of MGs. For example, Tong et al. found that the local changes in the connected network of atoms are the main driving force of rejuvenation in MGs by combining experiments and molecular dynamics (MD) simulations [49]. In this

work, the effect of pressure preloading (from 0 to 50 GPa) on the rejuvenation of $Zr_{46}Cu_{46}Al_8$ MGs was studied by MD simulations. Here, we applied pressure in the process of glass-forming quenching, discussing the effects of the pressure-promoted rejuvenation process on Poisson's ratio, potential energy, defects, short range order and medium range order, thereby explaining the enhanced plastic performance of rejuvenated MGs. Our work sheds light on designing plastic MGs by weakening the medium range order and provides a more complete description of the relationship between pressure, rejuvenation, atomic structure and shear bands.

2. Simulation details

Based on the embedded atom method (EAM) potential developed by Cheng et al., MD simulations were performed in LAMMPS [50, 51]. In this work, the Zr-Cu-Al system was selected because of its reliable empirical potential and excellent glass-forming ability. The random $Zr_{46}Cu_{46}Al_8$ configuration was composed of 4600 Zr atoms, 4600 Cu atoms and 800 Al atoms. At 2000 K and zero pressure, the model was fully equilibrated for 1 ns under periodic boundary conditions (PBCs), within an NPT ensemble (constant number, constant pressure, and constant temperature) [52]. The Nose-Hoover thermostat and Parrinello-Rahman technique were adopted to control the temperature and pressure [53, 54]. The model was subjected to quenching to 50 K at a cooling rate of 10^{12} K/s at zero pressure. According to the kink in the volume–temperature curve, T_g was about 755 K. The pressure-promoted models were relaxed at 980 K (~1.3T_g) for 2 ns: 0 GPa, 10 GPa, 20 GPa, 30 GPa, 40 GPa and 50 GPa, respectively. These models were then quenched to 50 K at a cooling rate of 10^{12} K/s

under the corresponding pressure. Finally, they were relaxed at 50 K and zero pressure for 4 ns. The big MG models, containing 320,000 atoms (22.4×5.6×44.8 nm^3) were prepared by replicating the small models, and were subjected to a compressive strain rate of $4x10^7$/s along the Z-direction at 50 K. A PBC was enforced along the Y direction under zero pressure while both X- and Z- directions maintained free surfaces. The existence of free surfaces is the key factor in forming shear bands [55].

3. Results

3.1. Stress-strain curve

The stress-strain curves of the rejuvenated MGs prepared by different levels of pressure preloading are presented in Fig. 1. The results show that pressure preloading can significantly improve the deformation capability of MGs. The maximum stress and the curve slope of the MG without pressure preloading are both greater than those of rejuvenated MGs with pressure preloading. The larger the pressure, the smaller the maximum stress and the slope, corresponding to the smaller Young's modulus. The stress of the MG prepared under 50 GPa doesn't show a steep drop, and the stress-strain curve is almost linear after the maximum stress. The difference in the yield stress and the quasi-steady flow stress indicates the degree of softening in the deformation process, which reflects the tendency of strain localization. The lower strength drop of the rejuvenated MGs with pressure preloading indicates that the degree of strain localization is lower than that of the MG without pressure preloading. Therefore, the compressive plasticity of an MG can be increased by pressure preloading. Previous reports have shown that the sharp drop in stress after yielding is related to a single shear

band [56], which means that multiple shear bands can be formed by pressure preloading. The models prepared by pressure preloading have a lower elastic limit, which may be attributed to more zones being available for shear transformation. To verify this, the atomic local shear strains of the models are shown in Fig. 2.

3.2. Atomic local shear strain

According to the atomic local shear strain, the atoms of the MGs are presented with different colors, as shown in Fig. 2 [57]. It is generally believed that only atoms with local shear strain larger than 0.3 are considered to be involved in plastic deformation [58]. Different plastic deformation behaviour between the MGs with and without pressure preloading can be more clearly observed in Fig. 2a and 2f. More uniform deformation and smaller localized strain are observed in the MG under 50 GPa. From Fig. 2b to 2e, the directions of the shear bands of MGs under 0 ~ 40 GPa are all close to 45° and 135°, and some different characteristics are observed. As the pressure increases, not only is the degree of localization of shear bands in Fig. 2e weaker than that in Fig. 2b but also more deformation units can be activated. In Fig. 2f, high-density deformation units are observed in different regions of the rejuvenated $Zr_{46}Cu_{46}Al_8$ MG under 50 GPa. It is interesting to point out that these deformation units have more difficulty in forming shear bands that causes brittle fracture, as compared to the MG without pressure preloading. In the literature, it is reported that multiple deformation units are usually induced by the multi-axial stress states, such as nano-indentation or notched samples [59, 60]. But in this work, the multiple deformation units are observed under the uniaxial loading state. This is because the pressure results in more shear

transformation zones (STZs) at different locations, which can facililate a more uniform strain distribution and avoids stress localization. The presence of high density STZs reduces the yield strength and leads to enhanced plasticity for the rejuvenated MGs prepared by pressure preloading.

3.3. Poisson's ratio, free volume and atomic packing density

It has been confirmed experimentally that there are direct correlations among Poisson's ratio, free volume, atomic packing density and pressure [61, 62]. Poisson's ratio (ν) is the negative ratio of transverse shrinkage strain to the longitudinal expansion strain in the elastic load direction, which reflects the resistance of the material to volume change vs shape change. Therefore, Poisson's ratio can be used to estimate the change of free volume and density in the MGs after pressure treatment.

$$\nu = \left(3 - 2\frac{G}{B}\right)/\left(6 + 2\frac{G}{B}\right) \quad (1)$$

where G is the shear modulus and B is the bulk modulus. G and B can be derived from the stiffness coefficients (C_{ij}) through the standard equations for isotropic materials [63-65].

The free volume can be defined as the Voronoi volume less the atomic core volume [66]. The atomic core volume is generally a constant, so the difference of the average Voronoi volume (ΔV_a) in the pressured and as-cast MGs can represent the change of free volume. The positive value of ΔV_a represents the increase of the free volume, while the negative value of ΔV_a represents the decrease of the free volume.

$$\Delta V_a = V_{ap} - V_{aa} \quad (2)$$

where V_{ap} and V_{aa} are the averaged Voronoi volumes in the pressured and as-cast MGs.

The atomic packing density (C_g) can reflect the free volume in MGs, which is defined as the ratio of the minimum theoretical volume occupied by the atoms to the effective volume of the corresponding MG.

$$C_g = \frac{\sum_{i=1}^{3} \frac{4}{3}\pi\left(\frac{R_i}{2}\right)^3}{V} \quad (3)$$

where i=1, 2, 3 stand for the elements Zr, Cu and Al, respectively. R_i is the position of the first peak of the pair distribution function. V is the overall volume of the $Zr_{46}Cu_{46}Al_8$ MG sample.

As shown in Fig. 3, Poisson's ratio and the change of the average Voronoi volume are both positively related to the atomic packing density (Cg). As the pressure increases, Poisson's ratio and the average Voronoi volume both increase. This suggests that more and more free volume is retained in the rejuvenated MG because the free volume is difficult to be annihilated under pressure. Liu et al. found that under pressure, the free volume in MGs with high Poisson's ratio is hard to annihilate, meaning more STZs can be activated [61]. Pan found that the volume of the STZs increases with the increase of Poisson's ratio [67]. The STZs preferentially appear in regions with large free volume. More STZs strengthen the shear capacity, and many shear band nuclei are formed, as shown in Fig. 2f. Our results are consistent with the literature, verifying the reliability of our models.

3.4. Potential energy

There is also another parameter reflecting the correlation between the deformation and microstructure, namely the change of potential energy ΔE.

$$\Delta E = E_P - E_A \quad (4)$$

where E_A and E_P are the potential energies of MGs in the as-cast state and pressured state. ΔE is negative in the case of aging, while it is positive in the case of rejuvenation.

As shown in Fig. 4, the positive ΔE increases as the pressure increases, which suggests that pressure is helpful to the rejuvenation. From the view point of the potential energy landscape, possessing abundant minima on its multidimensional energy surface [68], physical aging promotes MGs to move from a high-energy state to a deeper energy minimum, resulting in a loss of energy and entropy. Conversely, the pressure brings MGs into the high-energy areas, increasing the inherent structural energy. The increase in energy can cause instability of the atomic motion, which in turn changes the concentration of defects in MGs. In order to grasp the distribution of the defects density overall, the quasi-nearest atoms (QNAs) were considered. Each face of the Voronoi polyhedron, identifying the nearest neighbors to each atom in the MGs, corresponds to one of the nearest neighbors to the central atom. When two faces of a Voronoi polyhedron share an edge, the two corresponding atoms are called a pair of adjacent atoms. If the pair of adjacent atoms is not the nearest neighbor, the pair of adjacent atoms is called a pair of QNAs [69]. QNAs can be used to characterize defects in MGs. As shown in Fig. 4, when the pressure increases, the QNA increases, suggesting that the defects increase in rejuvenated $Zr_{46}Cu_{46}Al_8$ MGs. The above shows that pressure promotes an increase of the energy in MGs, accompanied by an increase in the defects.

3.5. Pair distribution function

In order to verify whether the rejuvenated $Zr_{46}Cu_{46}Al_8$ MGs are still completely amorphous, the pair distribution function (PDF) was analyzed. Fig. 5a shows the PDF

for MGs prepared by pressure preloading under 0, 10, 20, 30, 40, and 50 GPa. The results show that the structure of the rejuvenated $Zr_{46}Cu_{46}Al_8$ MGs is still amorphous. The position, width and strength of the peaks can reflect structural information. The atomic configurations of the nearest-neighbour shell make up the first peak of the PDF, corresponding to the short range order (SRO). The splitting of the second peak of the PDF is related to the polyhedral connection, corresponding to the medium range order (MRO) [70]. As shown in Fig. 5b, Gaussian fitting analysis was performed for the first and second peaks of the MGs with pressure preloading under 0 and 50 GPa. The first and second peaks of MGs with different pressure preloadings are different, which suggests that the pressure changes the degree of the SRO and MRO of rejuvenated $Zr_{46}Cu_{46}Al_8$ MGs. The first peak of the MG prepared by pressure preloading under 0 GPa is stronger than that under 50 GPa, while the second peak is just the opposite. This suggests that the pressure preloading may increase the degree of SRO but decreases the MRO. In order to verify this, the atomic structures of MGs under different pressures were analyzed.

3.6. Bonded pairs

The bonded pairs index with four integers *ijkl* is used to analyze the effect of pressure on the structure of MGs [71]. The first number *i* is used to determine if two atoms are bonded (*i*=1 for bonded pairs and *i*=2 for non-bonded pairs); *j* is the number of nearest neighbor atoms shared by two bonded atoms; *k* is the number of bonds among common neighbor atoms; when the three integers *ijk* are the same, *l* represents the difference in the geometry of the bonds. To further analyze the structural information

contained in the bonded pairs, the bonded pairs can be divided into two categories: when the common neighbor atoms are connected to form a closed ring, that is, when $k=j$, they are called "saturated bonded pairs"; otherwise, they are "unsaturated bonded pairs"[55]. As shown in Fig. 6a, when the pressure increases, the number of saturated bonded pairs (such as 1551, 1661 and 1441) increase, whereas unsaturated bonded pairs (such as 1431 and 1541) decrease. Fig. 6a also shows a group of fragmented bonded pairs composed of various low-population bonded pairs, which have a lower symmetry and lower energy barrier to shear transitions. The number of fragmented bonded pairs also decrease as the pressure increases. Besides the geometry of the bonded pairs, the bonded length was also calculated, as shown in Fig. 6b. As the pressure increases, the overall bonded length decreases. The above means that the bonded characteristic of the rejuvenated $Zr_{46}Cu_{46}Al_8$ MGs with pressure preloading has been changed from the low-symmetry to the high-symmetry levels, accompanied by a decrease of the bonded length. The atomic structure is remarkably mediated by virtue of pressure and is identified in detail by the Voronoi polyhedra analysis in the following.

3.7. Short range order

The Voronoi polyhedra (VP) can be described using the Voronoi index $<n_3, n_4, n_5, n_6>$, where n_i represents the number of i-edged faces [72]. Fig. 7 shows the distribution of the top 4 VP of $Zr_{46}Cu_{46}Al_8$ MGs with different pressure preloading values, where the element types are not distinguished. There is also a group of fragmented VP composed of various low-population VP, which have low symmetry and a low barrier to shear deformation [63]. As the pressure increases, the <0,0,12,0>, <0,2,8,1> and

<0,2,8,2> VP increase, while the fragmented VP decrease. The decrease of the fragmented VP can increase the barriers to shear deformation, making MGs difficult to achieve high density STZs. Besides the fragmented VP, the <0,0,12,0> VP are also selected as the representative polyhedra for analysis. The <0,0,12,0> VP, corresponding to full icosahedra, are strongly correlated with the shear deformation of MGs [73]. A larger yield strength was observed for higher icosahedra content, associated with the enhanced shear resistance compared to other types of SRO [56]. The <0,0,12,0,> VP increased from 8.13% to 10.49% when the pressure increased from 0 to 50 GPa. Other researchers also found that the MGs after the pressure adjustment are in a high energy state, accompanied by the increase of atomic packing and icosahedral SRO [47, 74]. The increase of <0,0,12,0,> VP also can increase shear resistance, making MGs difficult to achieve high density STZs. However, as shown in Fig. 2f, more uniform deformation and smaller localized strain are observed in the $Zr_{46}Cu_{46}Al_8$ MG under 50 GPa. The above shows that the SRO is not effective in explaining the role of pressure in promoting the deformation of the rejuvenated $Zr_{46}Cu_{46}Al_8$ MGs, so a higher order structure is needed, that is, the MRO.

3.8. Medium range order

The MRO is related to the polyhedral connection. The neighboring polyhedra can be connected by sharing one, two, three or four atoms, which corresponds to sharing one vertex, one edge, one face and one flattened tetrahedron [75, 76]. The connectivity of the <0,0,12,0> VP and other main VP was analyzed because of their close relationship with shear deformation [73, 77]. As shown in Fig. 8, as the pressure

increases, the connectivity between <0,0,12,0> VP and the other main VP, such as <0,2,8,1>, <0,0,12,0>, <0,2,8,2> and <0,2,8,0>, is weakened. Combined with Fig. 7, although the number of icosahedra in the rejuvenated MGs is much larger than that in ordinary MGs, the interrelation between the icosahedra and other polyhedra is weakened. The pressure-induced rejuvenation increases the SRO but decreases the MRO that usually has a high shear resistance [78, 79], which suggests that the MGs under pressure preloading have low resistance to deformation. Therefore, the high energy of the rejuvenated $Zr_{46}Cu_{46}Al_8$ MGs is mainly attributed to the pressure-promoted weakening of the MRO.

Fig. 9 shows the different connections of <0,0,12,0> and other VP under different pressures, depending on how many atoms are shared between them. As the pressure increases, the number of polyhedra connected by *3-atom* decreases, while those connected by *2-atom* and *4-atom* increase in the rejuvenated MGs. The number of polyhedra connected by *1-atom* hardly changes with pressure, so it's not shown. The number of *3-atom* connections increases while the number of *2-atom* and *4-atom* connections reduces in the MG, relative to the liquid [73, 76, 80]. It demonstrates that with the increase of pressure, the rejuvenated MG is closer to the liquid. Ding et al. also found that slow cooling rates can lead to more orderly structures, accompanied by increase of the *3-atom* connections and decrease of the *2-atom* and *4-atom* connections [76]. This means that the number of *3-atom* connections increases at the cost of the *2-atom* and *4-atom* connections, and they can switch between each other. In other words, the number of *2-atom* and *4-atom* connections increases at the cost of the *3-atom*

connections in the rejuvenated $Zr_{46}Cu_{46}Al_8$ MGs, reducing the structural ordering. So the structural feature of weakening the *3-atom* cluster connections can represent an increase in the rejuvenation level.

4. Discussion

The propensity of a region to shear deformation depends mainly on its local microstructure. In terms of microstructure, the enhanced plasticity performance of rejuvenated $Zr_{46}Cu_{46}Al_8$ MGs arises from the increase of the QNA and the decrease of the MRO. This is because the pressure preloading reduces the ability of an atom to diffuse by reducing the removable space. At the same time, Poisson's ratio in the elastic range is almost linear with the atomic packing density. So, the main influence of pressure on the deformation units is in nucleation rather than growth. The pressure reconstructs the atomic configuration and forces the stress of the deformation units to a level below the stress of the overall failure, favoring a homogeneous deformation. So, the rejuvenated $Zr_{46}Cu_{46}Al_8$ MGs with the weakening MRO, possess high density, high energy, high Poisson's ratio, high defects and low localization, as shown in Fig. 10.

In detail, different polyhedral connections can result in different stiffnesses of the local structures. For instance, Ding et al. found that polyhedra with *3-atom* connections show the stiffest elastic response during the shear deformation [76]. The fraction of *3-atom* connections in the rejuvenated $Zr_{46}Cu_{46}Al_8$ MGs decreases with the increasing pressure, leading to the decrease of stiffness in local regions. The number of *2-atom*s and *4-atom*s connections increases, suggesting that the local structure is more prone to deformation. Therefore, many shear band nuclei are formed in regions with numerous

of *2-atom* and *4-atom* connections, due to these connections behaving in a more flexible manner. From the view point of energy, *3-atom* connections can lead to a higher energy barrier of the basin in the potential energy landscape, and an increase of the shear modulus [81]. Therefore, the decrease of *3-atom* connections leads to lowering the energy barrier and the stiffness for shear deformation. In addition, the pressure-promoted MGs are already in a high energy state, so the low activation energy of local plastic units leads to more STZs being activated. As the strain increases, the STZs coalesce, interact and branch. The distribution of local shear strain is more uniform, leading to enhanced plasticity.

5. Conclusions

The effects of pressure preloading on the microstructure and plasticity of $Zr_{46}Cu_{46}Al_8$ MGs were investigated. New design strategies can be achieved for improving the deformation capability in MGs via the pressure preloading approach. The larger the pressure, the smaller the maximum stress and Young's modulus. In terms of microstructure, the enhanced plasticity performance of $Zr_{46}Cu_{46}Al_8$ MGs arises from the increase of the QNA and the decrease of the MRO. The number of the *2-atom* and *4-atom* connections increases at the cost of the *3-atom* connections of the icosahedra and other VP in the rejuvenated $Zr_{46}Cu_{46}Al_8$ MGs. The decrease of *3-atom* connections can lower the energy barrier and the stiffness for shear deformation, improving the level of rejuvenation. This can lead to more STZs being activated in the rejuvenated and high-energy $Zr_{46}Cu_{46}Al_8$ MGs. The rejuvenated $Zr_{46}Cu_{46}Al_8$ MGs, with the weakened MRO, possess high density, high energy, high Poisson's ratio, high defects and low

localization. The results obtained give improved understanding in the rejuvenation mechanisms of MGs prepared by pressure preloading and are expected to provide guidance in the design of MGs with enhanced plasticity.

Acknowledgments

This work was supported by the Hong Kong Scholars Program (Grant No. XJ2017049), the Hong Kong Polytechnic University (Grant No. G-YZ1J), the National Natural Science Foundation of China (Grant No. 51801174) and the Program for the Top Young Talents of Higher Learning Institutions of Hebei (Grant No. BJ2018021). LMW would like to acknowledge the support from the National Basic Research Program of China (Grant No. 2015CB856805).

Data availability

The raw/processed data required to reproduce these findings cannot be shared at this time due to technical or time limitations.

References

[1] K.L. Edwards, E. Axinte, L.L. Tabacaru, A critical study of the emergence of glass and glassy metals as “green” materials, Mater. Des. 50 (2013) 713-723.

[2] E. Axinte, Glasses as engineering materials: A review, Mater. Des. 32(4) (2011) 1717-1732.

[3] T.C. Hufnagel, C.A. Schuh, M.L. Falk, Deformation of metallic glasses: Recent developments in theory, simulations, and experiments, Acta Mater. 109 (2016) 375-393.

[4] G. He, J. Eckert, W. Loser, L. Schultz, Novel Ti-base nanostructure-dendrite composite with enhanced plasticity, Nat. Mater. 2(1) (2003) 33-37.

[5] P. Tandaiya, R. Narasimhan, U. Ramamurty, On the mechanism and the length scales involved in the ductile fracture of a bulk metallic glass, Acta Mater. 61(5) (2013) 1558-1570.

[6] E. Axinte, Metallic glasses from “alchemy” to pure science: Present and future of

design, processing and applications of glassy metals, Mater. Des. 35 (2012) 518-556.

[7] H.Y. Song, J.J. Xu, Y.G. Zhang, S. Li, D.H. Wang, Y.L. Li, Molecular dynamics study of deformation behavior of crystalline Cu/amorphous $Cu_{50}Zr_{50}$ nanolaminates, Mater. Des. 127 (2017) 173-182.

[8] J.C. Qiao, Y. Yao, J.M. Pelletier, L.M. Keer, Understanding of micro-alloying on plasticity in $Cu_{46}Zr_{47-x}Al_7Dy_x$ ($0 \leq x \leq 8$) bulk metallic glasses under compression: Based on mechanical relaxations and theoretical analysis, Int. J. Plast. 82 (2016) 62-75.

[9] J.M. Pelletier, D.V. Louzguine Luzgin, S. Li, A. Inoue, Elastic and viscoelastic properties of glassy, quasicrystalline and crystalline phases in $Zr_{65}Cu_5Ni_{10}Al_{7.5}Pd_{12.5}$ alloys, Acta Mater. 59(7) (2011) 2797-2806.

[10] J.C. Qiao, Y.J. Wang, J.M. Pelletier, L.M. Keer, M.E. Fine, Y. Yao, Characteristics of stress relaxation kinetics of $La_{60}Ni_{15}Al_{25}$ bulk metallic glass, Acta Mater. 98 (2015) 43-50.

[11] Z. Ning, W. Liang, M. Zhang, Z. Li, H. Sun, A. Liu, J. Sun, High tensile plasticity and strength of a CuZr-based bulk metallic glass composite, Mater. Des. 90 (2016) 145-150.

[12] L. Li, E.R. Homer, C.A. Schuh, Shear transformation zone dynamics model for metallic glasses incorporating free volume as a state variable, Acta Mater. 61(9) (2013) 3347-3359.

[13] Y.Q. Cheng, E. Ma, Atomic-level structure and structure-property relationship in metallic glasses, Prog. Mater. Sci. 56(4) (2011) 379-473.

[14] J.C. Qiao, J.M. Pelletier, Influence of thermal treatments and plastic deformation on the atomic mobility in $Zr_{50.7}Cu_{28}Ni_9Al_{12.3}$ bulk metallic glass, J. Alloys Compd. 615 (2014) S85-S89.

[15] K.K. Song, X.L. Han, S. Pauly, Y.S. Qin, K. Kosiba, C.X. Peng, J.H. Gong, P.X. Chen, L. Wang, B. Sarac, S. Ketov, M. Mühlbacher, F. Spieckermann, I. Kaban, J. Eckert, Rapid and partial crystallization to design ductile CuZr-based bulk metallic glass composites, Mater. Des. 139 (2018) 132-140.

[16] X.H. Sun, Y.S. Wang, J. Fan, H.J. Yang, S.G. Ma, Z.H. Wang, J.W. Qiao, Plasticity improvement for dendrite/metallic glass matrix composites by pre-deformation, Mater. Des. 86 (2015) 266-271.

[17] J. Pan, Y.X. Wang, Q. Guo, D. Zhang, A.L. Greer, Y. Li, Extreme rejuvenation and softening in a bulk metallic glass, Nat. Commun. 9(1) (2018) 560.

[18] Y. Fan, T. Iwashita, T. Egami, How thermally activated deformation starts in metallic glass, Nat. Commun. 5 (2014) 5083.

[19] M. Wakeda, J. Saida, J. Li, S. Ogata, Controlled rejuvenation of amorphous metals with thermal processing, Sci. Rep. 5 (2015) 10545.

[20] P. Ross, S. Küchemann, P.M. Derlet, H. Yu, W. Arnold, P. Liaw, K. Samwer, R. Maaß, Linking macroscopic rejuvenation to nano-elastic fluctuations in a metallic glass, Acta Mater. 138 (2017) 111-118.

[21] J. Saida, R. Yamada, M. Wakeda, S. Ogata, Thermal rejuvenation in metallic glasses, Sci. Technol. Adv. Mater. 18(1) (2017) 152-162.

[22] H.R. Lashgari, J.M. Cadogan, D. Chu, S. Li, The effect of heat treatment and cyclic loading on nanoindentation behaviour of FeSiB amorphous alloy, Mater. Des. 92 (2016) 919-931.

[23] J. Ding, Y.Q. Cheng, H. Sheng, M. Asta, R.O. Ritchie, E. Ma, Universal structural parameter to quantitatively predict metallic glass properties, Nat. Commun. 7 (2016) 13733.

[24] S.D. Feng, L. Qi, F.L. Zhao, S.P. Pan, G. Li, M.Z. Ma, R.P. Liu, A molecular dynamics analysis of internal friction effects on the plasticity of $Zr_{65}Cu_{35}$ metallic glass, Mater. Des. 80 (2015) 36-40.

[25] S.V. Ketov, Y.H. Sun, S. Nachum, Z. Lu, A. Checchi, A.R. Beraldin, H.Y. Bai, W.H. Wang, D.V. Louzguine-Luzgin, M.A. Carpenter, A.L. Greer, Rejuvenation of metallic glasses by non-affine thermal strain, Nature 524(7564) (2015) 200-203.

[26] S.V. Madge, D.V. Louzguine-Luzgin, A. Kawashima, A.L. Greer, A. Inoue, Compressive plasticity of a La-based glass-crystal composite at cryogenic temperatures, Mater. Des. 101 (2016) 146-151.

[27] D. Grell, F. Dabrock, E. Kerscher, Cyclic cryogenic pretreatments influencing the

mechanical properties of a bulk glassy Zr-based alloy, Fatigue Fract. Eng. Mater. Struct. 41(6) (2018) 1330-1343.

[28] W. Guo, R. Yamada, J. Saida, Rejuvenation and plasticization of metallic glass by deep cryogenic cycling treatment, Intermetallics 93 (2018) 141-147.

[29] Y. Tong, W. Dmowski, H. Bei, Y. Yokoyama, T. Egami, Mechanical rejuvenation in bulk metallic glass induced by thermo-mechanical creep, Acta Mater. 148 (2018) 384-390.

[30] H.B. Ke, P. Wen, H.L. Peng, W.H. Wang, A.L. Greer, Homogeneous deformation of metallic glass at room temperature reveals large dilatation, Scripta Mater. 64(10) (2011) 966-969.

[31] M. Zhang, Y.M. Wang, F.X. Li, S.Q. Jiang, M.Z. Li, L. Liu, Mechanical relaxation-to-rejuvenation transition in a Zr-based bulk metallic glass, Sci. Rep. 7(1) (2017) 625.

[32] D.V. Louzguine-Luzgin, V.Y. Zadorozhnyy, S.V. Ketov, Z. Wang, A.A. Tsarkov, A.L. Greer, On room-temperature quasi-elastic mechanical behaviour of bulk metallic glasses, Acta Mater. 129 (2017) 343-351.

[33] R. Raghavan, K. Boopathy, R. Ghisleni, M.A. Pouchon, U. Ramamurty, J. Michler, Ion irradiation enhances the mechanical performance of metallic glasses, Scripta Mater. 62(7) (2010) 462-465.

[34] S. Hóbor, A. Révész, P.J. Szabó, A.P. Zhilyaev, V.K. Kis, J.L. Lábár, Z. Kovács, High pressure torsion of amorphous $Cu_{60}Zr_{30}Ti_{10}$ alloy, J. Appl. Phys. 104(3) (2008) 033525.

[35] Y. Cao, X. Xie, J. Antonaglia, B. Winiarski, G. Wang, Y.C. Shin, P.J. Withers, K.A. Dahmen, P.K. Liaw, Laser shock peening on Zr-based bulk metallic glass and its effect on plasticity: experiment and modeling, Sci. Rep. 5 (2015) 10789.

[36] W. Dmowski, Y. Yokoyama, A. Chuang, Y. Ren, M. Umemoto, K. Tsuchiya, A. Inoue, T. Egami, Structural rejuvenation in a bulk metallic glass induced by severe plastic deformation, Acta Mater. 58(2) (2010) 429-438.

[37] F.Q. Meng, K. Tsuchiya, Seiichiro, Y. Yokoyama, Reversible transition of deformation mode by structural rejuvenation and relaxation in bulk metallic glass,

Appl. Phys. Lett. 101(12) (2012) 121914.

[38] L. Krämer, V. Maier-Kiener, Y. Champion, B. Sarac, R. Pippan, Activation volume and energy of bulk metallic glasses determined by nanoindentation, Mater. Des. 155 (2018) 116-124.

[39] H.J. Jin, X.J. Gu, P. Wen, L.B. Wang, K. Lu, Pressure effect on the structural relaxation and glass transition in metallic glasses, Acta Mater. 51(20) (2003) 6219-6231.

[40] Y. Fang, J. Jiang, High-pressure effects on Ti–Zr–Ni metallic glass and its corresponding quasicrystal, J. Non-Cryst. Solids 358(23) (2012) 3212-3215.

[41] F. Ye, K. Lu, Pressure effect on crystallization kinetics of an Al–La–Ni amorphous alloy, Acta Mater. 47(8) (1999) 2449-2454.

[42] Z. Wang, S. Scudino, K.G. Prashanth, J. Eckert, Corrosion properties of high-strength nanocrystalline $Al_{84}Ni_7Gd_6Co_3$ alloy produced by hot pressing of metallic glass, J. Alloys Compd. 707 (2017) 63-67.

[43] P. Yu, H.Y. Bai, J.G. Zhao, C.Q. Jin, W.H. Wang, Pressure effects on mechanical properties of bulk metallic glass, Appl. Phys. Lett. 90(5) (2007) 051906.

[44] A.R. Yavari, A.L. Moulec, A. Inoue, N. Nishiyama, N. Lupu, E. Matsubara, W.J. Botta, G. Vaughan, M.D. Michiel, Å. Kvick, Excess free volume in metallic glasses measured by X-ray diffraction, Acta Mater. 53(6) (2005) 1611-1619.

[45] Y.C. Hu, P.F. Guan, Q. Wang, Y. Yang, H.Y. Bai, W.H. Wang, Pressure effects on structure and dynamics of metallic glass-forming liquid, J. Chem. Phys. 146(2) (2017) 024507.

[46] C. Wang, Z.Z. Yang, T. Ma, Y.T. Sun, Y.Y. Yin, Y. Gong, L. Gu, P. Wen, P.W. Zhu, Y.W. Long, X.H. Yu, C.Q. Jin, W.H. Wang, H.Y. Bai, High stored energy of metallic glasses induced by high pressure, Appl. Phys. Lett. 110(11) (2017) 111901.

[47] J. Ding, M. Asta, R.O. Ritchie, Anomalous structure-property relationships in metallic glasses through pressure-mediated glass formation, Phys. Rev. B 93(14) (2016) 140204(R).

[48] Q. Zeng, Z. Zeng, H. Lou, Y. Kono, B. Zhang, C. Kenney-Benson, C. Park, W.L. Mao, Pressure-induced elastic anomaly in a polyamorphous metallic glass, Appl.

Phys. Lett. 110(22) (2017) 221902.

[49] Y. Tong, T. Iwashita, W. Dmowski, H. Bei, Y. Yokoyama, T. Egami, Structural rejuvenation in bulk metallic glasses, Acta Mater. 86 (2015) 240-246.

[50] Y.Q. Cheng, E. Ma, H.W. Sheng, Atomic level structure in multicomponent bulk metallic glass, Phys. Rev. Lett. 102(24) (2009) 245501.

[51] S. Plimpton, Fast parallel algorithms for short-range molecular dynamics, J. Comput. Phys. 117(1) (1995) 1-19.

[52] W.G. Hoover, Canonical dynamics: equilibrium phase-space distributions, Phys. Rev. A 31(3) (1985) 1695.

[53] M. Parrinello, A. Rahman, Polymorphic transitions in single crystals: A new molecular dynamics method, J. Appl. Phys. 52(12) (1981) 7182-7190.

[54] S. Nosé, A unified formulation of the constant temperature molecular dynamics methods, J. Chem. Phys. 81(1) (1984) 511-519.

[55] S.D. Feng, L. Qi, L.M. Wang, S.P. Pan, M.Z. Ma, X.Y. Zhang, G. Li, R.P. Liu, Atomic structure of shear bands in $Cu_{64}Zr_{36}$ metallic glasses studied by molecular dynamics simulations, Acta Mater. 95 (2015) 236-243.

[56] A.J. Cao, Y.Q. Cheng, E. Ma, Structural processes that initiate shear localization in metallic glass, Acta Mater. 57(17) (2009) 5146-5155.

[57] F. Shimizu, S. Ogata, J. Li, Theory of shear banding in metallic glasses and molecular dynamics calculations, Mater. Trans. 48(11) (2007) 2923-2927.

[58] Z.D. Sha, Q.X. Pei, V. Sorkin, P.S. Branicio, Y.W. Zhang, H.J. Gao, On the notch sensitivity of CuZr metallic glasses, Appl. Phys. Lett. 103(8) (2013) 081903.

[59] B. Wei, T. Zhang, L. Zhang, D. Xing, W. Li, Y. Liu, Plastic deformation in Ce-based bulk metallic glasses during depth-sensing indentation, Mater. Sci. Eng., A 449 (2007) 962-965.

[60] J. Pan, Y.X. Wang, Y. Li, Ductile fracture in notched bulk metallic glasses, Acta Mater. 136 (2017) 126-133.

[61] X.F. Liu, R.J. Wang, W.H. Wang, Poisson's ratio of metallic glasses under pressure and low temperature, Scripta Mater. 62(5) (2010) 254-257.

[62] T. Rouxel, H. Ji, T. Hammouda, A. Moreac, Poisson's ratio and the densification

of glass under high pressure, Phys. Rev. Lett. 100(22) (2008) 225501.

[63] Y.Q. Cheng, A.J. Cao, E. Ma, Correlation between the elastic modulus and the intrinsic plastic behavior of metallic glasses: The roles of atomic configuration and alloy composition, Acta Mater. 57(11) (2009) 3253-3267.

[64] G. Duan, M.L. Lind, M.D. Demetriou, W.L. Johnson, W.A. Goddard III, T. Çağin, K. Samwer, Strong configurational dependence of elastic properties for a binary model metallic glass, Appl. Phys. Lett. 89(15) (2006) 151901.

[65] T. Çain, J.R. Ray, Third-order elastic constants from molecular dynamics: Theory and an example calculation, Phys. Rev. B 38(12) (1988) 7940.

[66] Q.K. Li, M. Li, Free volume evolution in metallic glasses subjected to mechanical deformation, Mater. Trans. 48(7) (2007) 1816-1821.

[67] D. Pan, A. Inoue, T. Sakurai, M.W. Chen, Experimental characterization of shear transformation zones for plastic flow of bulk metallic glasses, Proc. Natl. Acad. Sci. USA 105(39) (2008) 14769-14772.

[68] F.H. Stillinger, A topographic view of supercooled liquids and glass formation, Science 267(5206) (1995) 1935-1939.

[69] S.P. Pan, S.D. Feng, J.W. Qiao, W.M. Wang, J.Y. Qin, Correlation between local structure and dynamic heterogeneity in a metallic glass-forming liquid, J. Alloys Compd. 664 (2016) 65-70.

[70] J. Ding, E. Ma, Computational modeling sheds light on structural evolution in metallic glasses and supercooled liquids, npj Comput. Mater. 3(1) (2017) 9.

[71] J.D. Honeycutt, H.C. Andersen, Molecular dynamics study of melting and freezing of small Lennard-Jones clusters, J. Phys. Chem. 91(19) (1987) 4950-4963.

[72] N. Medvedev, The algorithm for three-dimensional Voronoi polyhedra, J. Comput. Phys. 67(1) (1986) 223-229.

[73] J. Ding, Y.Q. Cheng, E. Ma, Full icosahedra dominate local order in $Cu_{64}Zr_{34}$ metallic glass and supercooled liquid, Acta Mater. 69 (2014) 343-354.

[74] N. Miyazaki, M. Wakeda, Y.J. Wang, S. Ogata, Prediction of pressure-promoted thermal rejuvenation in metallic glasses, npj Comput. Mater. 2(1) (2016) 16013.

[75] W.K. Luo, H.W. Sheng, E. Ma, Pair correlation functions and structural building

schemes in amorphous alloys, Appl. Phys. Lett. 89(13) (2006) 131927.

[76] J. Ding, E. Ma, M. Asta, R.O. Ritchie, Second-nearest-neighbor correlations from connection of atomic packing motifs in metallic glasses and liquids, Sci. Rep. 5 (2015) 17429.

[77] J. Ding, S. Patinet, M.L. Falk, Y. Cheng, E. Ma, Soft spots and their structural signature in a metallic glass, Proc. Natl. Acad. Sci. USA 111(39) (2014) 14052.

[78] M. Wakeda, Y. Shibutani, Icosahedral clustering with medium-range order and local elastic properties of amorphous metals, Acta Mater. 58(11) (2010) 3963-3969.

[79] M.Z. Li, C.Z. Wang, S.G. Hao, M.J. Kramer, K.M. Ho, Structural heterogeneity and medium-range order inZr_xCu_{100-x} metallic glasses, Phys. Rev. B 80(18) (2009) 184201.

[80] S.P. Pan, J.Y. Qin, W.M. Wang, T.K. Gu, Origin of splitting of the second peak in the pair-distribution function for metallic glasses, Phys. Rev. B 84(9) (2011) 092201.

[81] W.L. Johnson, M.D. Demetriou, J.S. Harmon, M.L. Lind, K. Samwer, Rheology and ultrasonic properties of metallic glass-forming liquids: A potential energy landscape perspective, MRS Bull. 32(8) (2007) 644-650.

Figure captions

Fig. 1. Stress-strain curves of rejuvenated $Zr_{46}Cu_{46}Al_8$ MGs under different pressures.

Fig. 2. Atomic local shear strain of rejuvenated $Zr_{46}Cu_{46}Al_8$ MGs at macrostrain 10% under the pressure (a) 0 GPa, (b) 10 GPa, (c) 20 GPa, (d) 30 GPa, (e) 40 GPa and (f) 50 GPa.

Fig. 3. Poisson's ratio ν and the difference of the average Voronoi volume ΔV_a of rejuvenated $Zr_{46}Cu_{46}Al_8$ MGs under different pressures. $\Delta V_a = V_{ap} - V_{aa}$, where V_{ap} and V_{aa} are the averaged Voronoi volume in the pressured and as-cast MGs.

Fig. 4. Quasi-nearest atom (QNA) and the change of potential energies (ΔE) in rejuvenated $Zr_{46}Cu_{46}Al_8$ MGs under different pressures.

Fig. 5. Pair distribution function of rejuvenated $Zr_{46}Cu_{46}Al_8$ MGs under different pressures.

Fig. 6 Bonded pairs and bonded length of rejuvenated $Zr_{46}Cu_{46}Al_8$ MGs under different pressures

Fig. 7. The distributions of Voronoi polyhedra, corresponding to short range order.

Fig. 8. Medium range order of icosahedra and other Voronoi polyhedra formed by their central atoms.

Fig. 9. The percent of connected clusters of <0,0,12,0> and other Voronoi polyhedra, for three cluster connections (*2-atom*, *3-atom* and *4-atom,* as shown in the insert) under different pressures.

Fig. 10. Schematic description of the effect of pressure on rejuvenation.

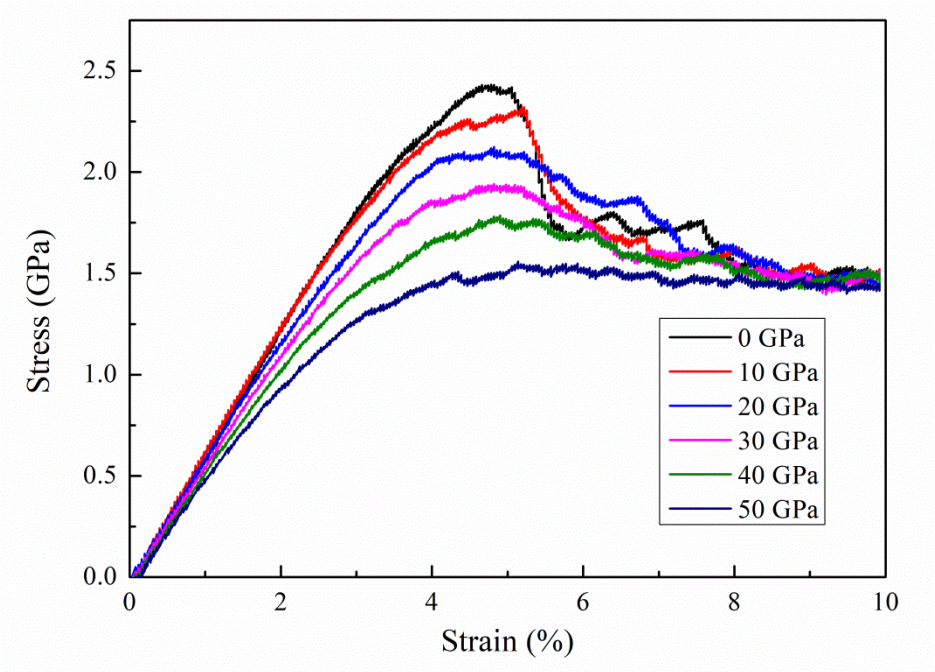

Fig. 1. Stress-strain curves of rejuvenated $Zr_{46}Cu_{46}Al_8$ MGs under different pressures.

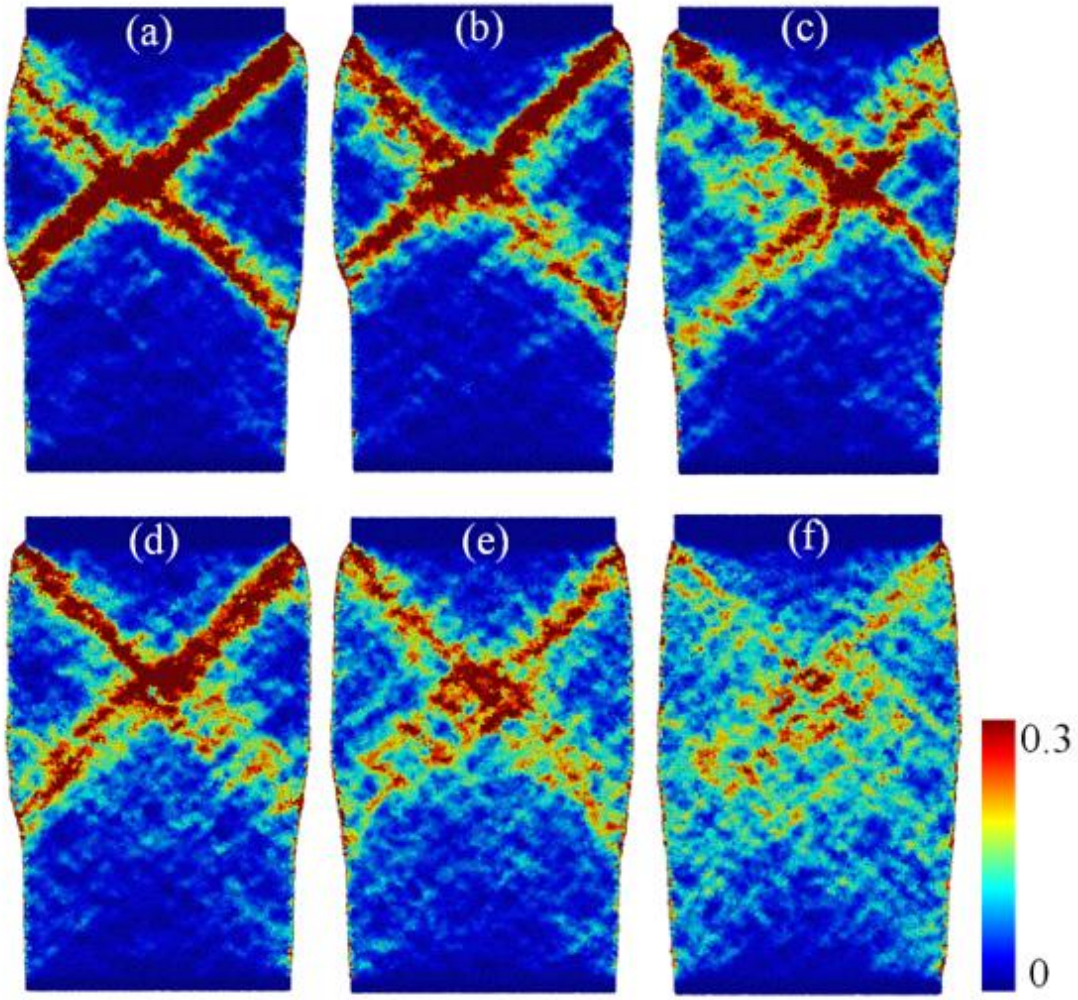

Fig. 2. Atomic local shear strain of rejuvenated $Zr_{46}Cu_{46}Al_8$ MGs at macrostrain 10% under the pressure (a) 0 GPa, (b) 10 GPa, (c) 20 GPa, (d) 30 GPa, (e) 40 GPa and (f) 50 GPa.

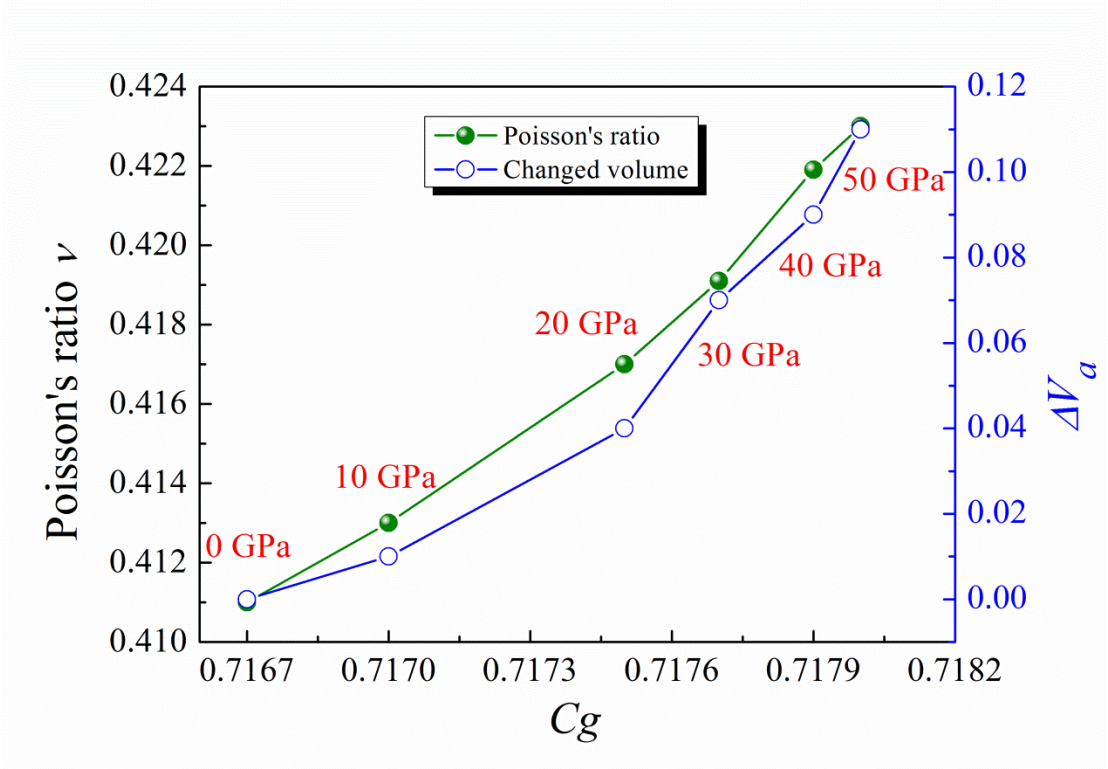

Fig. 3. Poisson's ratio ν and the difference of the average Voronoi volume ΔV_a of rejuvenated $Zr_{46}Cu_{46}Al_8$ MGs under different pressures. $\Delta V_a = V_{ap} - V_{aa}$, where V_{ap} and V_{aa} are the averaged Voronoi volume in the pressured and as-cast MGs.

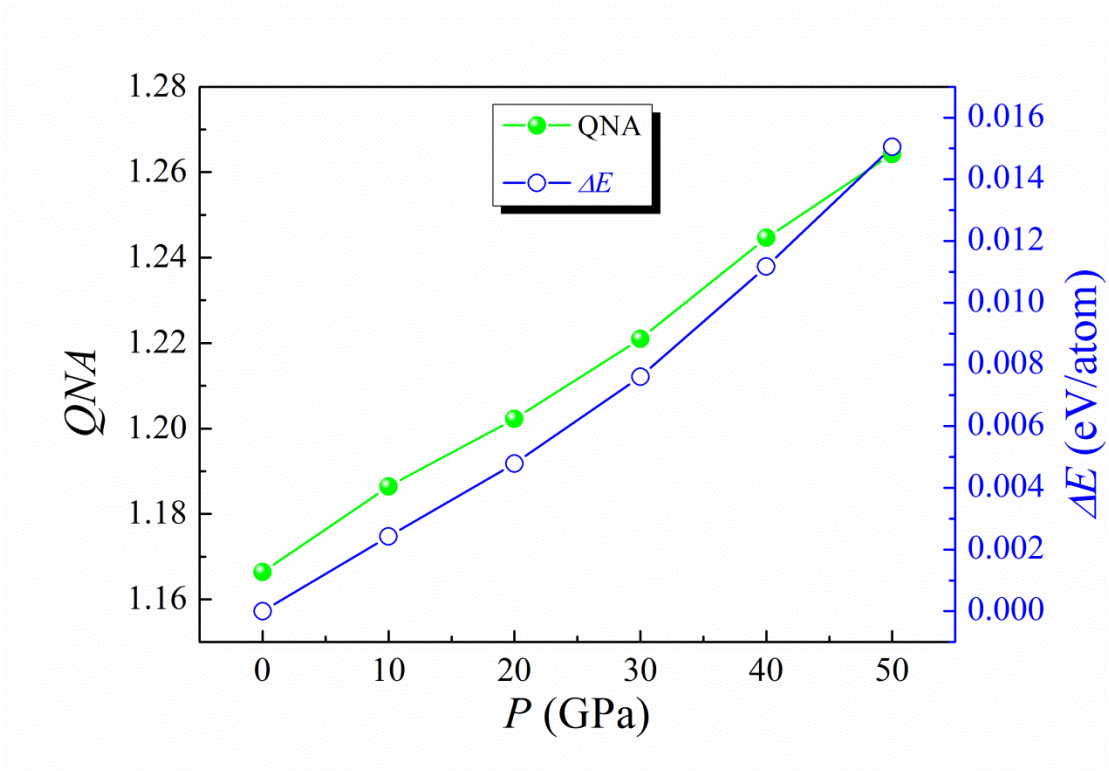

Fig. 4. Quasi-nearest atom (QNA) and the change of potential energies (ΔE) in rejuvenated $Zr_{46}Cu_{46}Al_8$ MGs under different pressures.

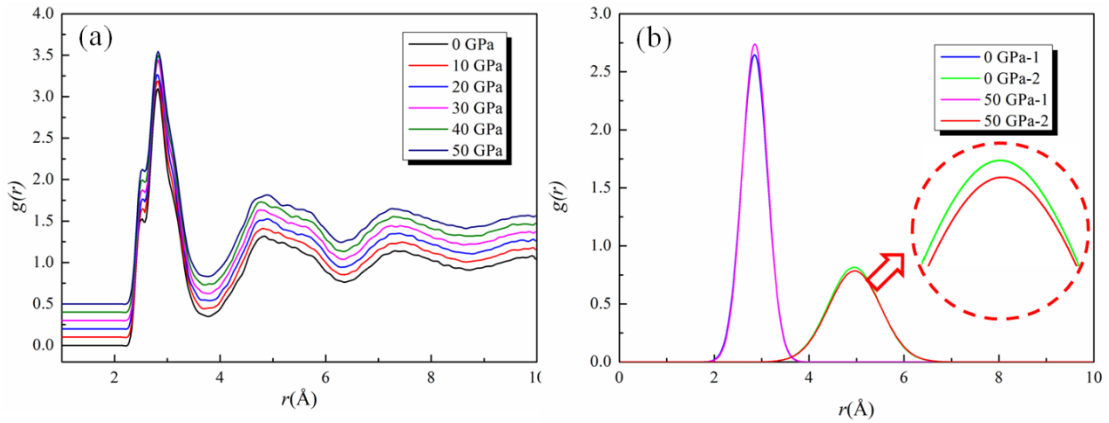

Fig. 5. (a) Pair distribution function of rejuvenated $Zr_{46}Cu_{46}Al_8$ MGs under different pressures. (b) Gaussian fitting analysis for the first and second peaks of MGs with pressure preloading under 0 and 50 GPa.

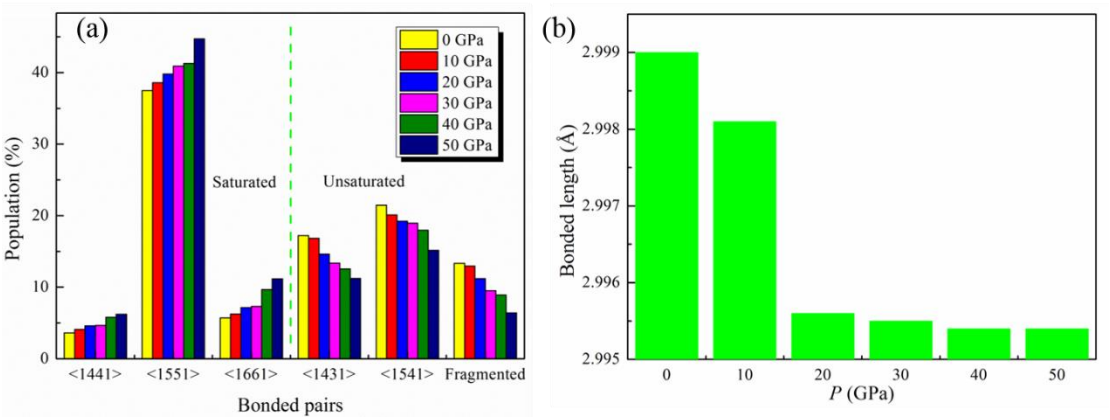

Fig. 6 Bonded pairs and bonded length of rejuvenated $Zr_{46}Cu_{46}Al_8$ MGs under different pressures.

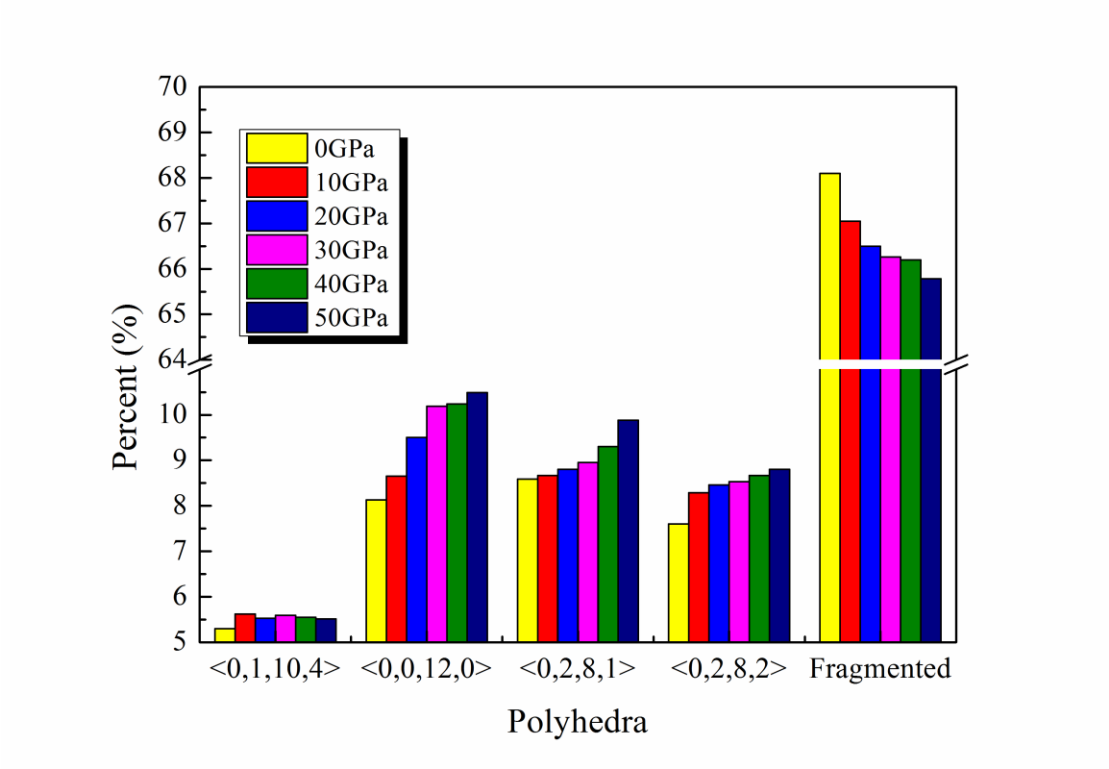

Fig. 7. The distributions of Voronoi polyhedra, corresponding to short range order.

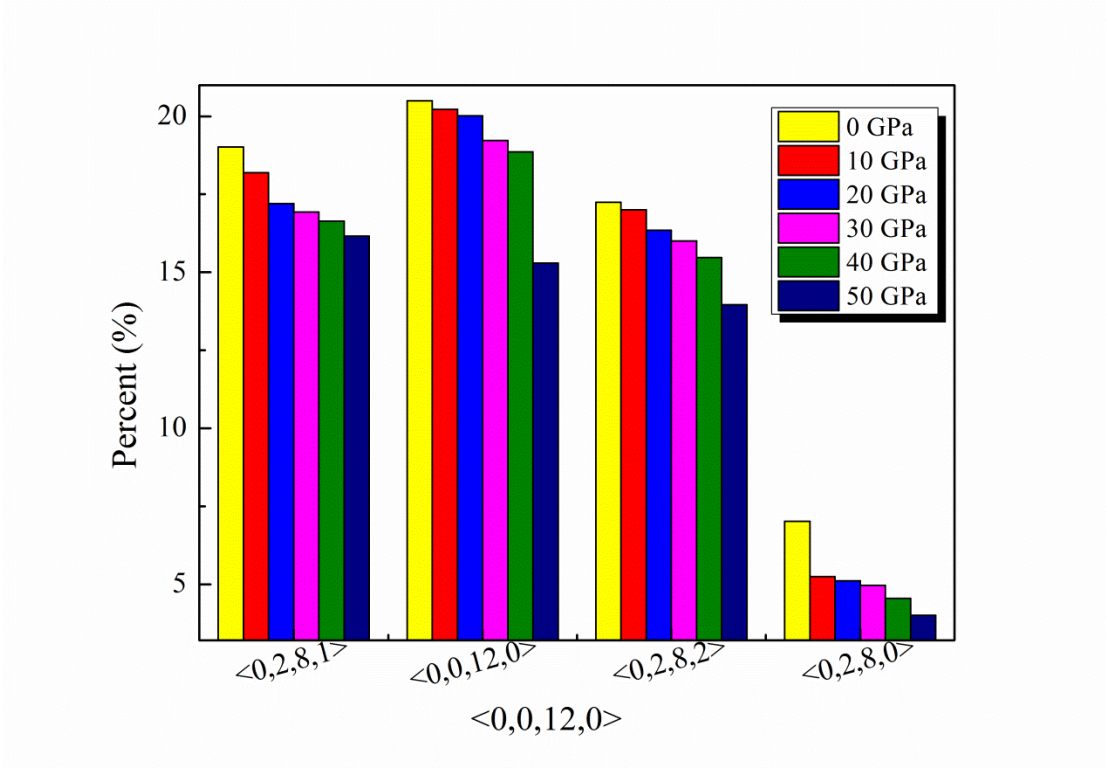

Fig. 8. Medium range order of icosahedra and other Voronoi polyhedra formed by their central atoms.

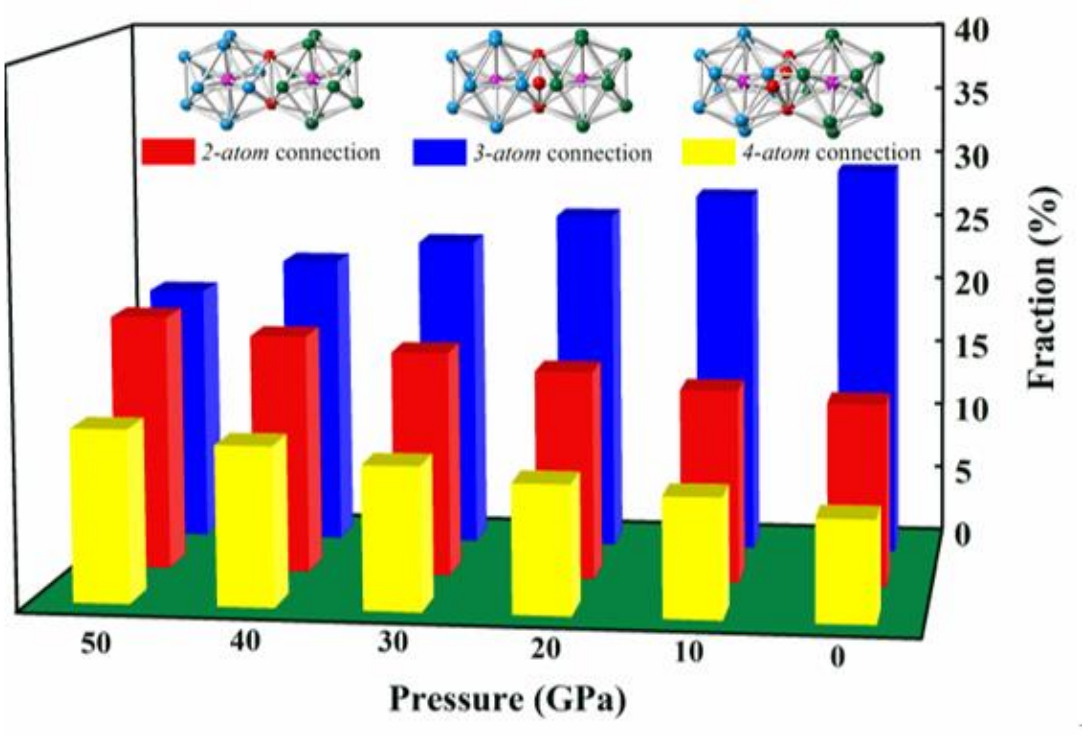

Fig. 9. The percent of connected clusters of <0,0,12,0> and other Voronoi polyhedra, for three cluster connections (*2-atom*, *3-atom* and *4-atom,* as shown in the insert) under different pressures.

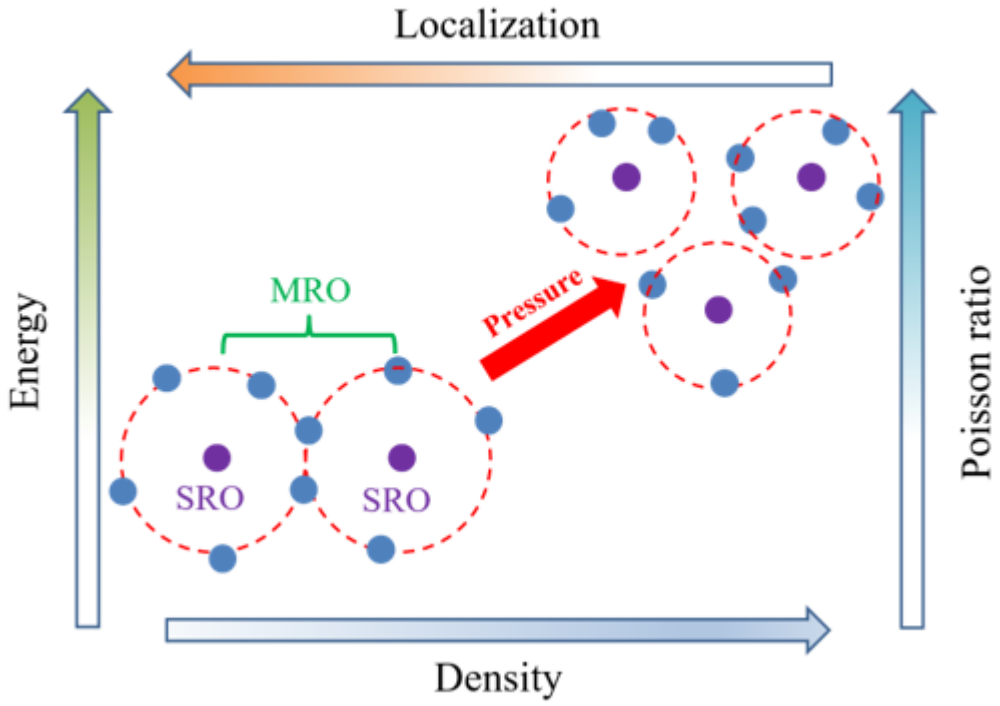

Fig. 10. Schematic description of the effect of pressure on rejuvenation.